Applied Catalysis A: General xxx (2008) xxx–xxx

Contents lists available at ScienceDirect

Applied Catalysis A: General

journal homepage: www.elsevier.com/locate/apcata

Bimetallic Pt-Metal catalysts for the decomposition of methanol: Effect of secondary metal on the oxidation state, activity, and selectivity of Pt

Jason R. Croy [a], S. Mostafa [a], L. Hickman [a], H. Heinrich [a,b], B. Roldan Cuenya [a,*]

[a] Department of Physics, University of Central Florida, Orlando, FL 32816, United States
[b] Center of Advanced Materials Processing and Characterization, University of Central Florida, Orlando, FL 32816, United States

ARTICLE INFO

Article history:
Received 14 June 2008
Received in revised form 9 August 2008
Accepted 17 August 2008
Available online xxx

Keywords:
Pt nanoparticles
Micelles
Pt-oxides
XPS
AFM
TEM
Mass spectrometry
Packed-bed mass flow reactor
Methanol decomposition
Bimetallic nanoparticles
Segregation
Catalysis

ABSTRACT

We present here a study of methanol (MeOH) decomposition over a series of bimetallic Pt-M catalysts, with M = Au, Pd, Ru, Fe. All samples have the same initial size distribution (~3 nm nanoparticle height), support (ZrO_2), and preparation conditions. Therefore, differences in the electronic and catalytic properties of the samples tested are related directly to the addition of the secondary metals (M). We find that the oxidation state as well as the activity of Pt is heavily influenced by the addition of the secondary metal. PtO is found to be highly stable in these systems and increasing concentrations of metallic Pt are associated with the surface segregation of metal M due to its affinity for the oxygen present during air annealing.

1. Introduction

Pt-Metal (Pt-M) bimetallic catalysts are important in a variety of applications ranging from fuel cells [1] to thermal coatings [2]. In addition, recent years have witnessed a surge in the interest of methanol (MeOH), especially as a potential storage fuel for hydrogen, ultimately used for the production of electricity in on-board applications such as the direct methanol fuel cell (DMFC), portable electronics, or stationary power generation. These applications potentially involve electro-oxidation, steam reforming, and the direct decomposition of MeOH, each encompassing unique reaction conditions [3].

In order to take advantage of Pt-M systems in the design of new catalysts for any of these applications, the structural, chemical, and electronic modifications, brought about by the addition of secondary metals [4–11], need to be fully understood. In particular, the surface compositions of such catalysts are influenced by a number of factors. Besides such familiar properties as surface energy, atomic volume, and heats of sublimation, nanoscale systems require additional considerations. For instance, it has been shown theoretically that Pt atoms may preferentially segregate to sites of low (edges, vertices, etc.) or high (facets) coordination depending on the structure of the particles as well as the metal M [12]. In addition, the presence of oxygen has been shown to heavily influence atomic segregation in nanoparticles (NPs), and the presence of metal M on the NP surface can affect the stability of oxide species on active nanocatalysts [13,14]. In reference to fuel cells, alloying Pt with metals such as Fe, Ru, Ni, Co, as well as others, has been reported to enhance the oxygen reduction reaction (ORR) [5,6], increase activity [15], and enhance resistance to CO poisoning [16]. In connection with the latter, Pt-Ru catalysts are known to be efficient and some detailed theoretical studies already exist concerning this catalyst's role in CO oxidation [17]. However, as stated earlier, these systems hold importance in a broader sense than power generation alone [18–32] and a large number of works

* Corresponding author.
E-mail address: roldan@physics.ucf.edu (B.R. Cuenya).

0926-860X/$ – see front matter © 2008 Elsevier B.V. All rights reserved.
doi:10.1016/j.apcata.2008.08.013

have been dedicated to understanding their synthesis, characterization, and catalytic properties [33–44]

Furthermore, with the ever increasing industrial use of nanomaterials, their impact on the environment has become an issue of great importance. Specifically, thermally or mechanically induced emissions of particulate Pt from automobile catalytic converters is a source of toxicological concern [45–48]. Therefore, not only are the activity, selectivity, and stability of the working catalysts important, but so also is the state in which they might be emitted into the environment upon reaction (oxidated, chlorinated, etc.). Although catalysts are prepared in a certain state (i.e. Pt^0), the oxidation state of the working catalyst might be different, and how this state evolves and reacts under environmental conditions is of interest.

In general, it is the surface properties of alloys which are credited with observed catalytic improvements, and as we will show in this article, the nature of the secondary metal, as well as the preparation and pretreatment conditions, have a large influence over the final composition and oxidation state of the surface and its active components. We present here an investigation of the influence that the addition of M = Au, Pd, Ru, and Fe has on the oxidation state, activity, and selectivity of supported $Pt_{0.8}M_{0.2}$ nanoparticles. We use as a probe reaction the decomposition of MeOH. Previous studies by our group [49,50] have shown that the size of Pt nanoparticle catalysts, as well as the particle support, can influence the type (PtO, PtO_2) and stability of the metal oxide shell present in "real-world" catalysts under realistic reaction conditions. Indeed, there has been recent interest in the role of oxidized versus metallic species in the activity of several systems where oxidized metals may contain some catalytic advantage [51,52]. To remove any ambiguities in the present study, we have used particles of the same average size for all samples and a common support, zirconia. Under these conditions the observed effects can be directly related to the addition of the secondary metal.

2. Experimental

Non-polar/polar diblock copolymers [poly(styrene)-block-poly(2vinylpyridine) Polymer Source Inc.] were dissolved in a non-polar solvent (toluene) in order to obtain spherical nano-cages (inverse micelles). These micelles were then loaded with metal salts ($H_2PtCl_6{\cdot}6H_2O$, $HAuCl_4{\cdot}3H_2O$, $RuCl_3$, $PdCl_2$, $FeCl_3$) to produce self-confined and size-selected Metal and Pt-Metal (Pt-M) NPs. The metal content of all bimetallic samples by weight (wt) was 80% Pt and 20% secondary metal. The particle size was controlled by using a polymer with a specific head length [PS(27700)-PVP(4300), i.e. constant PVP molecular weight for all samples] and by selecting a metal-salt/polymer-head (PVP) concentration for the solution of 0.2 for all samples [53–55]. The solution was then mixed with nanocrystalline ZrO_2 (~45 nm, Alfa Aesar) in the form of a powder. All samples were dried in air at ~100 °C for 24 h then placed in a tubular furnace, open to the air, for calcination at 500 °C for 2.5 h. Each catalyst sample had a total weight of 50 mg and contained 1% by weight metal.

The powder samples were transferred to an ultra high vacuum system (UHV, SPECS GmbH) for analysis by X-ray photoelectron spectroscopy (XPS). XPS data were collected using a monochromatic X-ray source (Al Kα, 1486.6 eV) operating at 350 W and a flood gun was used to correct for sample charging during measurement. All spectra were referenced to the Zr $3d_{5/2}$ [ZrO_2] peak at 182.6 eV [56].

Catalytic decomposition of methanol in the vapor phase was carried out in a packed-bed mass flow reactor with a vertical quartz tube (inner diameter = 4 mm) serving as the reactor vessel. A thermocouple (K-type) in contact with the reactor was used to monitor temperature and the entire assembly was insulated to minimize heat losses. Immediately prior to the reaction all catalysts were heated for 1 h at ~200 °C (below the initial calcination temperatures of 500 °C used to remove the polymeric nanoparticle shell) in a flow of He at 10 ml/min. Activities were measured at atmospheric pressure in the range of 100–220 °C. The composition of the feed was 0.05% MeOH relative to the flow of He, as determined by the partial pressures of He and the main fragment ion of MeOH (m/q = 31). Further details of the experimental set up and measurement conditions can be found in [49].

The polymer-salt solutions were also dip-coated on SiO_2/Si(0 0 1) substrates in order to obtain particle size information (height) via atomic force microscopy (AFM) with a Nanoscope Multimode (Digital Instruments) microscope operating in tapping mode. Transmission electron microscopy (TEM) was carried out on the powder samples with a Tecnai F30 TEM operating at an accelerating voltage of 300 kV. In addition, energy dispersive X-ray analysis (EDX) was conducted on each sample.

3. Results and discussion

3.1. Morphological and structural characterization

Fig. 1 displays representative images of the nanoparticle polymeric solutions dip-coated on SiO_2/Si(0 0 1). Here the three images show bimetallic samples [Pt-Au (a), Pt-Pd (b), and Pt-Fe (c)] before the removal of the polymeric shell. The images demonstrate the validity of our preparation method for the synthesis of bimetallic catalysts with narrow size distributions. Analysis of the images taken after the removal of the polymer (not shown), by heating in ultrahigh vacuum (UHV) for 30 min at 500 °C, gives an average particle size (height) of ~3 nm.

Fig. 2 shows elemental distribution maps of Pt (a) and Fe (b) obtained by TEM in the same region of the Pt-Fe sample. We can see a uniform distribution of the metals with Pt and Fe appearing in the same regions within a nanoparticle. Fig. 2(c) shows a faceted particle from the Pt-Au sample with a measured lattice parameter of 3.96 ± 0.02 Å. A pure Pt particle in a monometallic Pt sample with a lattice parameter of 3.74 ± 0.04 Å is displayed in Fig. 2(d). The lattice parameters for bulk Pt, bulk Au, and a $Pt_{0.8}Au_{0.2}$ alloy are 3.92, 4.07, and 3.94 Å, respectively [57,58]. Thus, our value of 3.96 Å for the Pt-Au particle is in agreement with the formation of a Pt-rich, Pt-Au alloy. The TEM images of Fig. 2 reveal our particles to be ~10 nm in diameter.

3.2. Electronic and chemical characterization

Figs. 3 and 4 show XPS spectra and Fig. 5 exhibits related compositional information for the monometallic Pt and Pt-M nanoparticle samples deposited on ZrO_2 powder. The fits were done after linear background subtraction using a product of Gaussian and Lorentzian functions, as defined in the software CASA XPS, with the maximum width (FWHM) of each component held constant [Pt^0 (1.8 eV), PtO (2.4 eV), PtO_2 (2.8 eV)] from spectrum to spectrum. The distinction of PtO and PtO_2 species, especially on small NPs, is difficult. An initial attempt to fit the Pt-4f region of our samples with only two doublets (one corresponding to Pt^0, the other to PtO_x) was made, but such a fit resulted in an unreasonably large FWHW (>3). Fig. 3 displays data from the Pt-4f core-level region. The vertical solid line in Fig. 3 marks the position of the $4f_{7/2}$ peak of metallic Pt at 71.7 eV. The two dashed lines represent the BEs of the $4f_{7/2}$ peaks of PtO and PtO_2 at 73.0 and 75.3 eV, respectively [59]. These reference values for PtO and PtO_2, as well as the energy difference between Pt^0 and PtO_2 (~3.6 eV), are

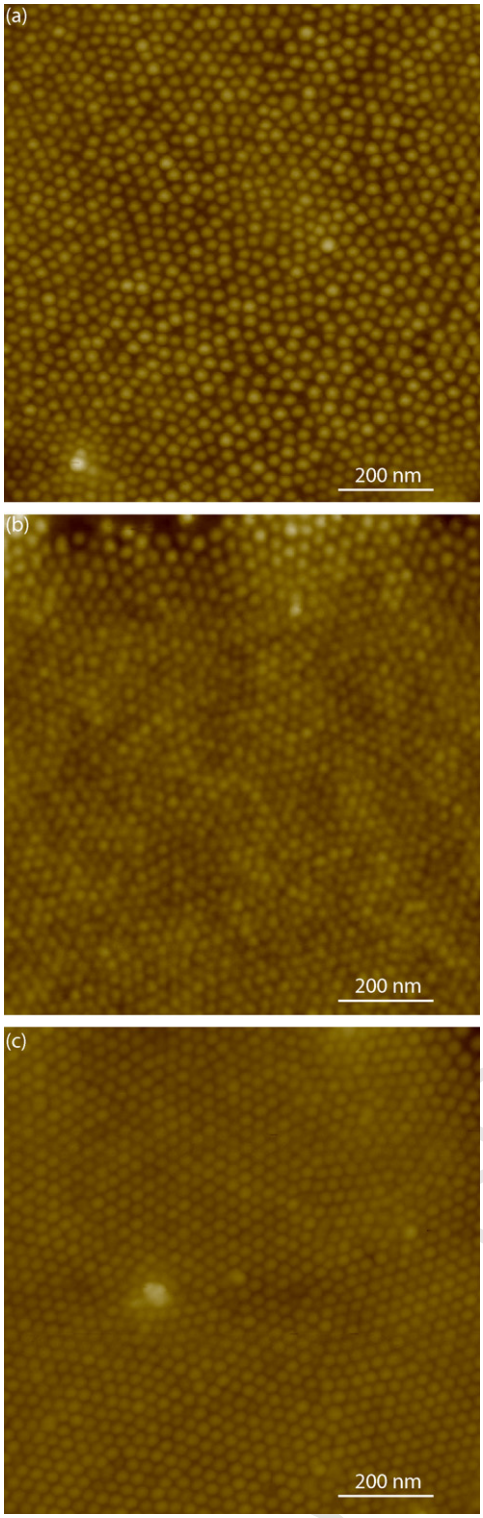

Fig. 1. AFM images of (a) Pt-Au, (b) Pt-Pd, and (c) Pt-Fe NPs (20% wt M) supported on SiO_2/Si(0 0 1). The images were taken before polymer removal.

consistent with several reports of supported Pt and Pt-M systems [60,61], as well as with preliminary data obtained by our group on similarly synthesized Pt NPs supported on thin film oxide surfaces after exposure to atomic oxygen in UHV and subsequent annealing. The Pt^0 $4f_{7/2}$ peak in our monometallic Pt NPs is shifted 0.6 eV higher than the value of bulk Pt [62]. This positive shift may be attributed to final state effects in our small clusters and/or an interaction with the support itself [63]. One possible interaction is the formation of interfacial Pt-Zr compounds. Alloying of Pt and Zr has been observed at 500 °C (our annealing temperature) [64] and the observed shift to higher binding energy of the Pt^0 $4f_{7/2}$ peak is in agreement with Ref. [65] as well as data from our group on the temperature-dependent reduction of ZrO_2-supported Pt NPs [66]. What effect these possible interfacial compounds have on the chemical properties of our systems will be investigated in more detail in the future. The relative content of the different Pt species and XPS binding energies obtained from the analysis of the data in Fig. 3 are summarized in Table 1. The estimated error in the fit of the area of the peaks is ±3%. An interesting trend appears in the concentration of Pt-oxides for these samples as shown in Fig. 5. The Pt-Au is the least metallic in composition being 22% Pt^0. As we go from Pt-Au to Pt-Pd we see a substantial increase in the amount of Pt^0. This increase continues as we go across Fig. 5 to Pt-Fe with a metallic Pt content of 60%.

Fig. 4 shows XPS spectra of the most intense photoelectron peaks associated with the secondary metals before and after the addition of Pt. The following core-level regions are shown in Fig. 4: (a) Au-4f, (b) Fe-2p, (c) Pd-3d (and ZrO_2-3p), and (d) Ru-3d. In Fig. 4(c) we can see that the Pd-3d region overlaps with the ZrO_2-3p substrate peaks and we have superimposed the Pd sample's spectrum on that of the ZrO_2 substrate's (bottom). The Pt-Pd sample is shown on top. Similarly for Ru, shown in Fig. 4(d), the Ru-3d region coincides with C-1s and a deconvolution has been done to identify the constituent components of the monometallic Ru (bottom) and the Pt-Ru (top) samples.

In order to better understand the segregation phenomena occurring in our bimetallic NPs during the post-synthesis annealing treatment in air at 500 °C, several fundamental properties of the monometallic metals should be kept in mind. For example, the order of decreasing size for the atomic radii (metallic and Wigner-Seitz) of our metals is Au > Pt > Pd > Ru > Fe [67,68]. The order of the heats of sublimation from high to low is Ru > Pt > Fe ∼ Pd > Au [69,70]. The surface energies from high to low go as Ru > Pt > Fe > Pd > Au [71] (experimental values). And finally, since our bimetallic NPs were annealed in the presence of oxygen (air), a parameter that should be taken into account is the heat of formation of the different oxides. Starting with the most stable oxide, the trend goes as Ru > Fe > Pd > Pt > Au [67].

Although all of the above trends refer to bulk systems, due to the relatively large size of our nanoparticles (∼10 nm in diameter) they are expected to be a reasonable referent for our studies. Theoretically it has been shown (for Cu-Ni systems) that clusters containing less than 1000 atoms are dominated by geometric effects, while those above this size are driven by thermodynamic effects reported for the macroscopic systems [72]. Using data from Ref. [12], a cubo-octahedral fcc Pt NP of 5 nm in diameter consists of at least 4000 atoms. Therefore, thermodynamic arguments of segregation given above should be valid. However, from the above parameters, the different affinities for oxygen of the distinct secondary metals are believed to play a key role. Alloys are notably affected by adsorbates from the surrounding gaseous environment and the metal having the highest affinity for these adsorbates will preferentially segregate to the surface [73,74]. This segregation effect has been observed, for example, in Pt-Rh catalysts [73]. There, the performance of the catalysts varied between pure Pt and pure Rh depending on the surface concentrations of each metal, with Rh preferentially occupying the surface under oxidizing conditions, and Pt under reducing conditions. We might note that many of the studies mentioned in Ref. [73] are on single crystals under controlled vacuum environments whereas our samples consist of multi-faceted, metal-oxide-supported, metallic nanoclusters. Because all of our samples have been prepared

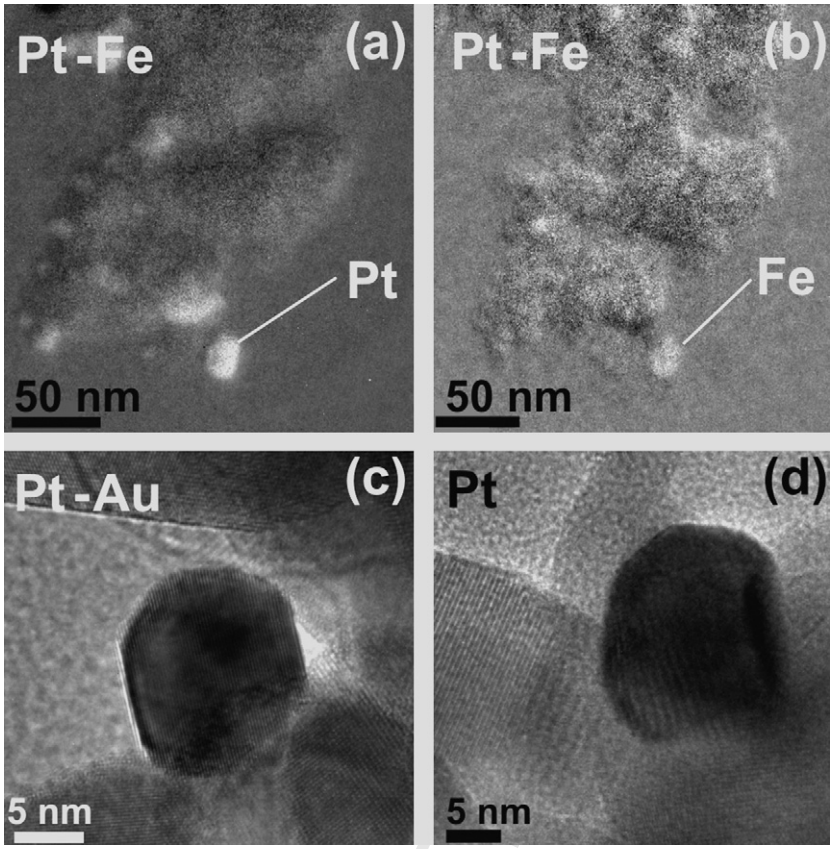

Fig. 2. (a) Elemental distribution map (using energy-filtered TEM) of the Pt-Fe NPs supported on ZrO_2 showing homogeneous distribution of Pt (a) and Fe (b) in individual clusters. (c) High resolution image of a particle in the Pt-Au sample and (d) a particle in the pure Pt sample.

under identical conditions, have similar size distributions, are on the same support (ZrO_2), and were calcined in air at the same temperature, the varying concentrations of the different Pt and PtO_x species (Table 1) must be related to the tendency of the secondary metals to segregate to the surface where oxygen is present during annealing. Therefore, larger amounts of PtO_x in our samples could be related to the presence of a larger number of superficial Pt atoms, while lower PtO_x/Pt^0 ratios would indicate that the secondary metal has segregated to the nanoparticle surface, minimizing Pt oxidation.

From the Pt-Au spectrum in Fig. 3, and Table 1, we see that the addition of Au seems to have had little effect on the oxidation state of Pt in this system as compared to the similarly prepared pure Pt NPs. The atomic radius of Au is larger than that of Pt so we would expect lattice strain to contribute to the segregation of Au to the NP surface. In addition, the surface energy and heat of sublimation of Au are each lower than the corresponding values for Pt, again promoting surface segregation of Au. It has also been shown theoretically that Au will segregate in a $Pt_{0.75}Au_{0.25}$ system [75], which is close to our $Pt_{0.8}Au_{0.2}$. However, Au does not have a high affinity for oxygen, and our annealing in air should not further favor the segregation of Au to the surface. The metallic state of Au in our pure Au and Pt-Au catalysts is confirmed in the Au-4f XPS spectra of Fig. 4(a). In Fig. 4(a), the Au $4f_{7/2}$ peak appears at 84.7 eV in the pure Au (bottom) NP sample, which is 0.7 eV higher than the value for bulk Au at 84.0 eV [76], and the same peak appears at 84.2 eV in the Pt-Au (top) sample (−0.5 eV shifted with respect to the pure Au NPs). For the latter sample we also see a negative shift in the binding energy of Pt^0 of 0.4 eV with respect to the pure Pt sample (Table 1). Bastl and Pick [77] have also reported negative binding energy shifts for both Pt and Au in Pt-Au alloys formed by vapor deposition of Au on polycrystalline Pt foils. Based on our XPS and TEM (average representation of the particle structure) data we conclude that the Pt-Au sample is a homogeneous nanoalloy with a slightly Au-rich surface. It is interesting to note that Zhang et al. [78] have reported that Au can stabilize Pt against dissolution in fuel cells by raising the oxidation potential of Pt, whereas in our Pt-Au system we do not find Pt to be reduced compared to the pure Pt sample. The authors point out that Au will interact differently when deposited on a metallic versus oxide substrate and that Au

Table 1
Relative phase content of the different Pt and Pt-oxide species as well as the binding energy of Pt^0 obtained from the Pt-4f XPS spectra shown in Fig. 3

Sample	Binding energy Pt^0 (eV)	Pt^0 content (%)	PtO content (%)	PtO_2 content (%)
Pt	71.7	28	63	9
Pt-Au	71.4	22	66	12
Pt-Au/MeOH	71.5	34	53	13
Pt-Pd	71.7	35	50	15
Pt-Ru	71.8	55	32	13
Pt-Fe	71.6	60	25	15

Also shown are the corresponding values of the Pt-Au sample after reaction with MeOH (spectrum in Fig. 9).

Please cite this article in press as: J.R. Croy, et al., Appl Catal A: Gen (2008), doi:10.1016/j.apcata.2008.08.013

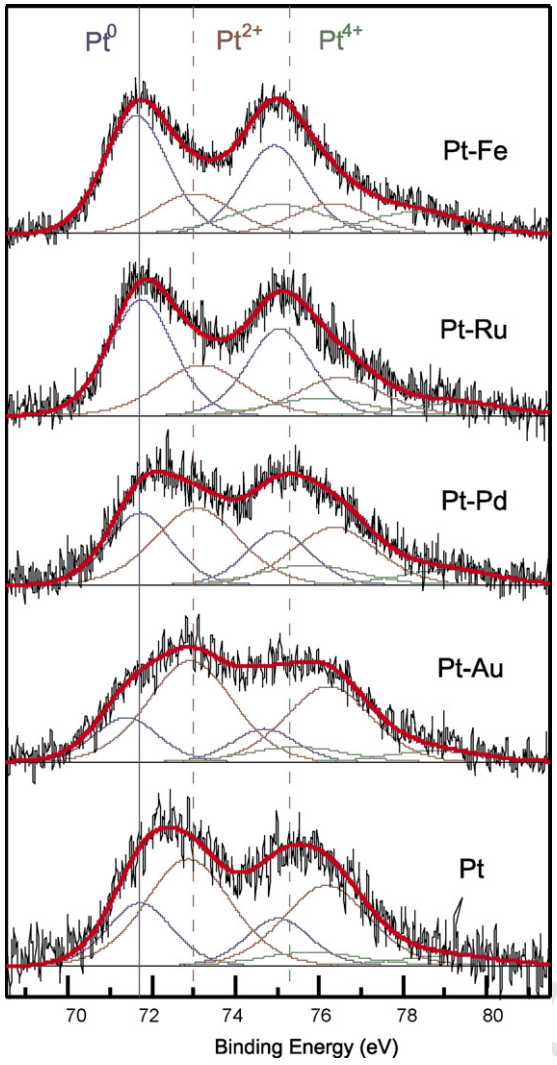

Fig. 3. XPS spectra of the Pt-4f region comparing monometallic Pt with bimetallic (Pt-M) NPs deposited on ZrO_2. From bottom to top, the Pt-M spectra reveal a trend of decreasing oxidation. The solid and dashed lines represent the $4f_{7/2}$ peaks of Pt^0, PtO and PtO_2, respectively.

deposited on Pt is unlikely to intermix with Pt. In our system we have evidence [TEM image shown in Fig. 2(c)] of the formation of a Pt-Au alloy, most likely due to our chemical synthesis method versus deposition of Au on a Pt (1 1 1) single crystal surface by Zhang et al. [78]. In addition our cluster diameters are roughly three times larger than their ~3 nm particles.

Since the surface energies of Pd and Fe are lower than that of Pt, and the heats of oxide formation of the former metals are higher, the segregation of Pd and Fe to the NP surface is expected. Anti-segregation has been predicted for Fe and a somewhat neutral behavior for Pd when these metals are alloyed with Pt in the absence of oxygen [75,79]. This emphasizes the importance of taking into account the affinity of the different metals for oxygen in understanding segregation phenomena in "real-world" nanocatalysts. In our samples, the segregation of Fe to the NP surface results in a Pt-rich core and a decrease in the amount of surface Pt-oxide compounds formed upon air annealing, as is seen in Table 1 and Figs. 3 and 5. From Fig. 4(b) we see the pure Fe NP sample (bottom) showing Fe^{2+} in FeO (after air annealing, 500 °C) at ~709 eV and the corresponding Pt-Fe (top) reveals Fe in the 3+ state (Fe_2O_3) at ~711.8 eV. The higher oxidation state of iron in the bimetallic sample suggests the possibility of Fe promoting the reduction of the Pt-oxide compounds that are formed in these particles. The results for the Pt-Fe sample are in qualitative agreement with a study by Niemantsverdriet et al. [80] who found Pt to be zero valent in an Fe-Pt alloy with the formation of Fe ions at the surface of the alloy particles.

The main XPS peaks of Pd-3d overlap with those of Zr-3p and could not be resolved in the Pt-Pd sample. However, the presence of PdO_x in the monometallic Pd sample can be inferred from the two shoulders visible in the Pd-3d region of Fig. 4(c). Here we see the spectrum of the monometallic Pd sample superimposed on the Zr-3p region of the substrate (bottom) and that of the Pt-Pd sample (top) with the solid and dashed vertical lines indicating the binding energies of the Pd^0 (335.9 eV, 341.2 eV) and Pd^{2+} (337.9 eV, 343.2 eV) 3d doublets, respectively. The peaks at ~333.1 and 346.6 eV correspond to the ZrO_2-3p substrate. In a study done by Graham et al. [81] on alumina-supported Pt-Pd catalysts, it was suggested that Pd on the surface of Pt-Pd alloys inhibited the formation of PtO_x. This might certainly be the case here in light of Pd's greater affinity for oxygen and the large amount of Pt^0 that was detected in this sample. Gu and Balbuena [13] have also shown theoretically that the incorporation of Pd, as well as Ru, into Pt decreases the stability of subsurface oxygen, especially in the case of Ru. These calculations agree with our observation that Pt-Ru contains less PtO than Pt-Pd, and both samples are more reduced in comparison to the monometallic Pt sample.

As seen in Fig. 4(d), the Ru-3d region overlaps with the C-1s region. However, upon deconvolution of the monometallic Ru spectrum (bottom) we uncover two states of oxidation, Ru^{6+} (RuO_3) at ~283 eV and Ru^{4+} (RuO_2) at ~281 eV. The peak at ~289 eV is a peak visible in the nanoparticle-free substrate (ZrO_2) spectrum and is attributed to a carboxylic species [82]. Analysis of the Pt-Ru sample (top) reveals the disappearance of the RuO_2 component (present in the monometallic Ru sample) at ~281 eV, and only the RuO_3 (~283 eV) remains. According to literature [67] RuO_2 should be the most stable oxide. However, analogous to the above discussion concerning Pt-Fe, the combination of Pt-Ru/ZrO_2 seems to favor the higher state of oxidation for Ru and possibly promotes the reduction of Pt.

From Ref. [12] we expect the surface atoms to be ~15% of the total number of atoms. Although it is possible for our $Pt_{0.8}M_{0.2}$ systems to form core-shell structures, the presence of PtO_x in all our samples leads us to conclude that we do not form such clusters.

3.3. Catalyst activity

Fig. 6 shows the rate of MeOH conversion (in units of μmol of MeOH/min/g cat) for each bimetallic Pt-M sample in the range of 150–220 °C. We mention here that no Pt-M catalysts achieved the same rate as the pure Pt sample which had a rate of ~4.5 μmol of MeOH/min/g cat at 200 °C (not shown). However, the pure Pd sample was comparable to pure Pt with an overall average rate of about 80% that of Pt, and the monometallic Ru sample was comparable to the Pt-Pd sample shown in Fig. 6. The monometallic Fe sample achieved a maximum activity of 31% that of Pt (220 °C) and the monometallic Au sample was not active in this temperature range.

Unexpected results were obtained while monitoring the reactivity of Pt-Ru and Pt-Pd samples. Pt-Ru alloys are generally accepted as being better catalysts than Pt alone, especially for use in fuel cells [79]. It is interesting that our Pt-Ru sample is relatively poor in comparison to our Pt-Au and Pt-Pd bimetallic samples, as shown in Fig. 6. This could be due to several factors. First of all, our

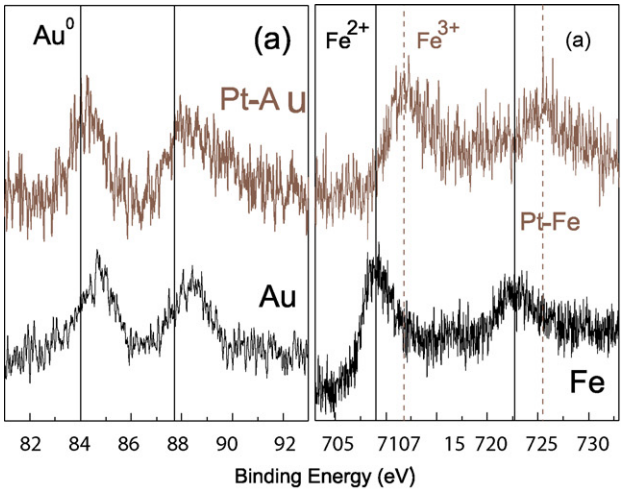

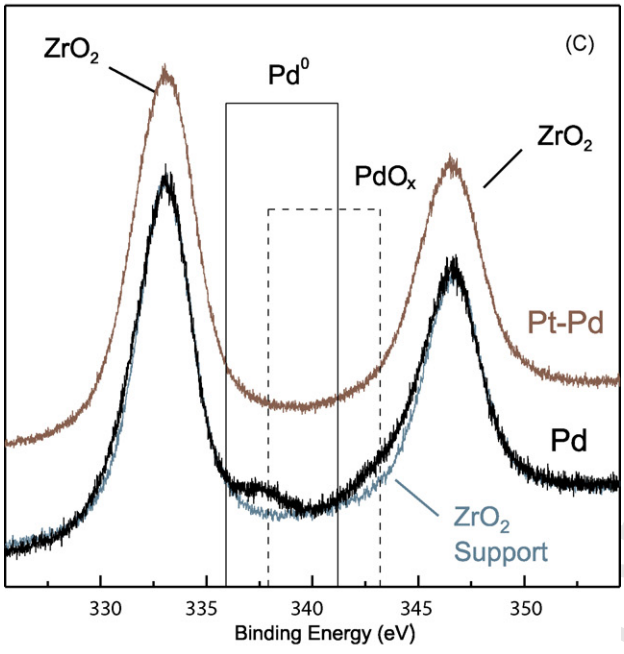

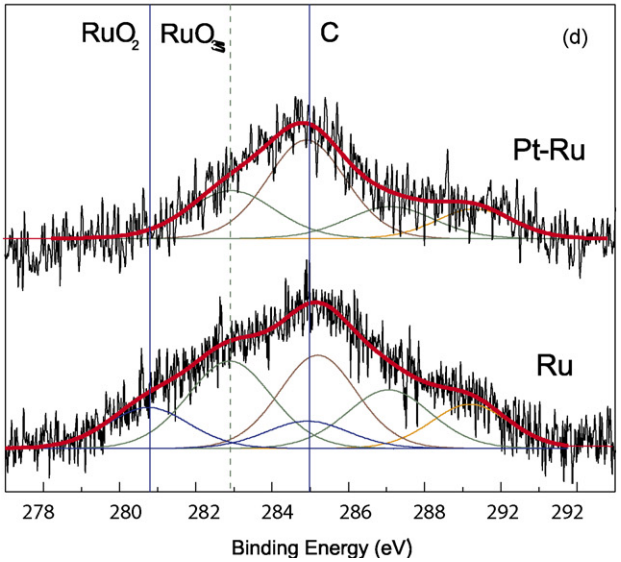

tests were not done in an electrochemical environment where we might expect reactions to proceed differently than in our gas-phase mass flow reactor. Waszczuk et al. [83] have also shown that MeOH behaves quite differently in UHV as compared to an electrochemical environment. Similarly, the rate of CO oxidation on Ru is much greater at higher oxygen coverages than under UHV conditions [84] and the selectivity for MeOH oxidation over a Ru catalyst is observed to be significantly different at low and high pressures [85]. Second, the concentration of the secondary metal is important and for Pt-Ru catalysts Pt:Ru concentrations of 3:1 and 1:1 are common [68]. Our Pt-Ru sample contains only 20% Ru and this low concentration might not be enough for the Pt to benefit from the presence of Ru.

The other point we would like to make note of concerns the Pt-Pd sample. Although both the monometallic Pt and Pd samples show high activity, the bimetallic Pt-Pd sample shows a decrease in activity with respect to both monometallic counterparts. In a recent paper by Zhang et al. [11] it was demonstrated that particles consisting of a monolayer of Pt covering a Pd/Co core showed high activity for O_2 reduction. The enhanced activity was partly attributed to lattice mismatch and a change in the d-band properties of Pt caused by interaction with Pd. In our case we imagine the reverse situation to be the prevailing one, in which Pd is enriched on the surface compared to Pt. It is feasible that the interaction of Pd with the underlying Pt is not as favorable as the geometry of Ref. [11], and that this interaction decreases the Pd activity towards MeOH decomposition. Further studies on this system should be carried out to answer this question.

Fig. 7 displays an Arrhenius plot [ln(Reaction Rate) versus $1/T$] for the Pt-M samples in the range of 190–220 °C. From this plot, activation energies (E_a) for MeOH decomposition can be obtained. The calculated activation energy for the monometallic Pt sample is 28 kJ/mol. The bimetallic E_a values are 59, 73, 96, and 89 kJ/mol for the Pt-Au, Pt-Pd, Pt-Ru, and Pt-Fe, respectively.

Fig. 8 correlates these data with the phase content (%) of Pt^0 (bottom axis) and PtO (top axis) in each Pt-M sample. The elemental labels denote the M in Pt-M nanocatalysts. For the y-axis we have calculated the percent difference of the rate for each sample, with respect to the monometallic Pt, at $T = 190$, 200, 210, and 220 °C, and plotted the average as:

$$\Delta R_{Pt}(\%) = \left\langle \frac{R_{Pt}(T) - R_{Pt-M}(T)}{R_{Pt}(T)} \times 100 \right\rangle$$

For example, the higher the average percent difference, the lower is the rate of MeOH conversion for a particular sample compared to the monometallic Pt. A clear trend emerges relating increasing amounts of metallic Pt with decreasing catalytic activity, and increasing amounts of PtO with increasing activity. The fits of the Pt-4f spectra in Fig. 3 show that only a small amount ($\leq$15%) of PtO_2 is present in our samples. Two factors may be discussed in connection with this trend: (i) the concentration of Pt^0 and PtO are related to the amount of surface segregation of M, as discussed in the XPS section; and (ii) PtO may play some role in the decomposition of MeOH. We will give only brief comments regarding (ii) as a detailed study on the stability of PtO under reaction conditions, and its catalytic reactivity for MeOH decomposition, is currently being conducted in our group and will be published elsewhere [86].

Fig. 4. XPS spectra of (a) Au-4f region of pure Au (bottom) and bimetallic Pt-Au NPs (top). (b) Fe-2p binding energy region of pure Fe (bottom) and bimetallic Pt-Fe NPs (top). (c) Pd-3d region of the monometallic Pd sample superimposed on the Zr-3p region of the substrate (bottom). The top spectrum shows the Pt-Pd sample. Two shoulders in the lower spectra reveal the presence of PdOx. (d) Ru-3d core-level region of the pure Ru (bottom) and bimetallic Pt-Ru (top) NP samples.

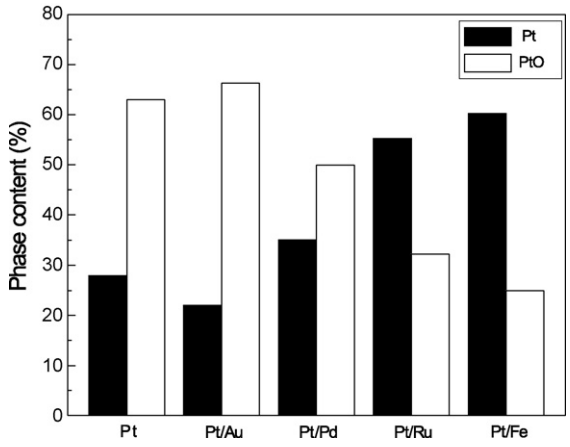

Fig. 5. Relative phase content (%) of Pt^0 and PtO in $Pt_{0.8}M_{0.2}$ NPs supported on ZrO_2 obtained from the XPS data in Fig. 3.

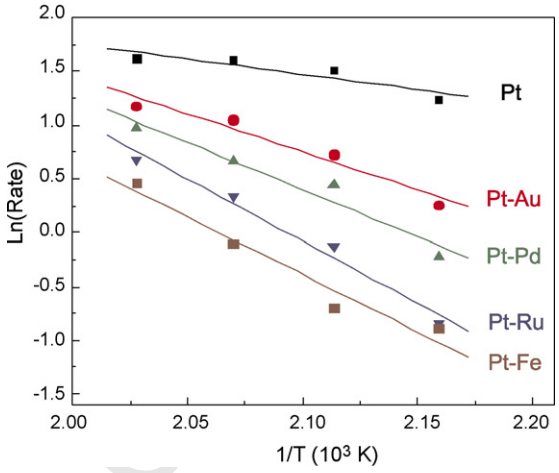

Fig. 7. Arrhenius plot of the methanol decomposition rate [ln(*R*) versus 1/*T*] over Pt-M NPs supported on ZrO_2.

3.4. Catalyst selectivity

Selectivity for each product gas is derived from the mass spectrometer data, along with stoichiometric considerations of the decomposition, water gas shift, and methanation reactions (Eqs. (3)–(5)), and is defined as the percentage of the total product that each particular partial gas pressure represents,

$$\text{Selectivity}\,(\%) = \frac{A_n}{\sum A_n} \times 100 \qquad (2)$$

where A_n represents the output of the *n*th product gas.

$$CH_3OH = CO + 2H_2 \qquad (3)$$

$$CO + H_2O = CO_2 + H_2 \qquad (4)$$

$$CO + 3H_2 = CH_4 + H_2O \qquad (5)$$

In the course of our experiments, only CO_2 and CH_4 were obtained as byproducts and only in small amounts at high temperatures. We can conclude from this that the reaction proceeds mainly through the direct decomposition of MeOH shown in equation (3). It is interesting to note that the Pt reference sample produced CO_2 at low temperatures (~2.5% at 150 °C). The amount of water in the experiment was ~0.2% as compared to the flow of the carrier gas He, which helps to facilitate reaction (4). This is in accord with the results of Iida and Igarashi [87] who reported high activity for the low temperature water gas shift reaction (WGS) on Pt/ZrO_2 catalysts. The authors were using a feed containing an H_2O to CO molar ratio of 5. The amount of water in our experiments is low compared to CO (~27%) since we are not directly introducing it into the feed, this will limit the occurrence of the WGS reaction in our experiments. None of the other samples showed this behavior for the WGS reaction at low temperatures. Bera et al. [88] have also reported Pt/CeO_2 active for the low temperature WGS reaction, with Pt being found mostly in the 2+ state (PtO). One interesting exception is the Ru sample which shows ~1% selectivity for CO_2 close to 300 °C. The corresponding Pt-Ru sample shows a switch to small amounts of CH_4 at the same temperature.

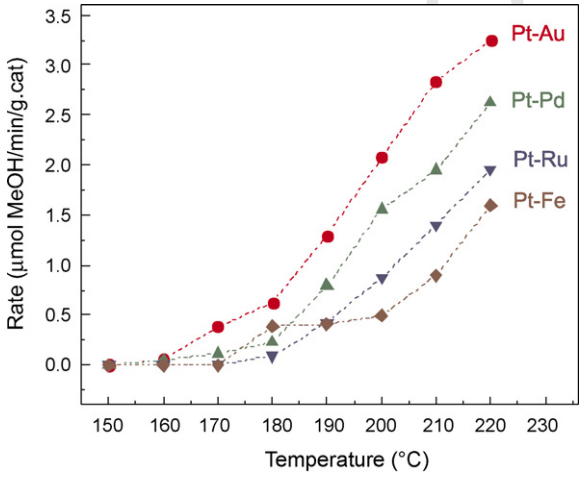

Fig. 6. Rate of MeOH decomposition given in µmol of MeOH/min/g cat for all bimetallic Pt-M samples in the temperature range of 190–220 °C.

4. Further discussion

4.1. Stability and reactivity of PtO

The monometallic Pt sample (Fig. 3, Table 1) is composed mainly of PtO (Pt^{2+}, 63%) as well as a fairly large (28%) contribution

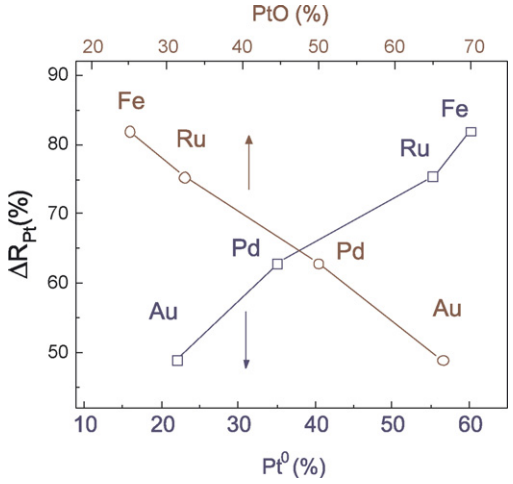

Fig. 8. Relative decrease in activity for Pt-M samples with respect to the monometallic Pt sample. The *y*-axis gives the average percent difference in the rate of MeOH decomposition in the range of 190–220 °C as explained in the text. The bottom and top *x*-axes relate this decrease to the concentration of Pt^0 and PtO, respectively. The elemental labels denote the M in Pt-M.

from the metallic component (Pt^0), with PtO_2 (Pt^{4+}) being considerably smaller (9%). The heats of oxide formation of PtO and PtO_2 [67] and theoretical calculations [89], indicate that PtO_2 should be the more stable oxide. However, possibly due to strong metal–support interactions, previously confirmed for this system [50], PtO is the most prevalent species under our preparation conditions. Interestingly, the most common terminations of Pt NPs are the (1 1 1) and (1 0 0) planes [90], for which it has been calculated that α-PtO_2 and PtO, respectively, are the most stable oxide phases [89]. However, new data from Seriani and Mittendorfer [91] have also shown that PtO_2 can be stable on the Pt(1 0 0) surface. Abe et al. [92] have also experimentally observed these phases to be stable up to 500 °C and the presence of large amounts of PtO might be related to the structure of our NPs. It has been reported for Pt single crystals that oxides can form at sites of low coordination (i.e. steps) where they are more stable than what is normally expected for bulk oxides [93]. Weaver et al. [94] have also observed enhanced thermal stability of oxides on Pt(1 1 1) due to the formation of three dimensional oxide particles accompanied by significant surface restructuring.

It is still not clear, even for bulk systems, which oxide species is the most stable, and NPs complicate the situation further because of their inherent complexity (i.e. high density of low coordinated sites, surface facets with different orientations, etc.) For example, Wang et al. [95] have observed experimentally that the surface oxide species that forms on Pt particles with diameters <1.3 nm is PtO_2, while above 2 nm, as in the case of our particles, PtO is observed. Oxide stability is observed in our bimetallic Pt-M systems with PtO being the most stable PtO_x species.

In Fig. 9 we show the Pt-4f core-level region of the Pt-Au sample before (bottom) and after (top) reaction with MeOH. The temperature ranged from 100 to 300 °C during the reaction with MeOH, and the total time on-stream was ~8 h. As we can see from Table 1, this sample is only moderately reduced under our reaction conditions and PtO is highly stable. More extreme H_2 reductions (not shown) were also carried out in our reactor with the same result that the PtO_x compounds could not be fully reduced. These samples were taken from the reactor and transferred in air to the UHV system where we still observed them to be reduced. Thus, complete re-oxidation does not occur during its exposure to air. However, this exposure during transfer is short (<10 min) and the initial air oxidation occurs at 500 °C. In addition to these experiments, preliminary data from *in situ* X-ray Absorption Near Edge Structure (XANES) measurements (not shown), acquired before and during long exposures (up to 10 h) of the pure Pt and Pt-Au catalysts to CO at various temperatures (up to 200 °C) at Brookhaven National Laboratory, reveal that the initial PtO_x compounds in these samples cannot be fully reduced [96], in agreement with our ex situ measurements of Fig. 9. Several interesting works have been published revealing the importance of oxides in catalytic systems [52,97–101] which lead to the question of whether or not PtO may play some role in the decomposition of MeOH. For example, in a recent paper by Li and Hammer [52], DFT calculations show that three-phase boundaries are particularly active sites for chemical reactivity. These boundaries involve the contact of the gas-phase reactants and products with the metallic and oxidized phases of the catalyst. Another example is the adsorption of MeOH on Cu which is greatly enhanced by the availability of oxygen [98], either from the feed gas or from the catalyst due to an incomplete reduction process [99]. Our XPS and reactor data associate increasing activity with increasing concentrations of PtO and the presence and stability of PtO in our catalysts reveal a novel aspect of these systems. However, one should keep in mind that the enhanced reactivity of the bimetallic NPs containing PtO may also be simply due to the higher content of

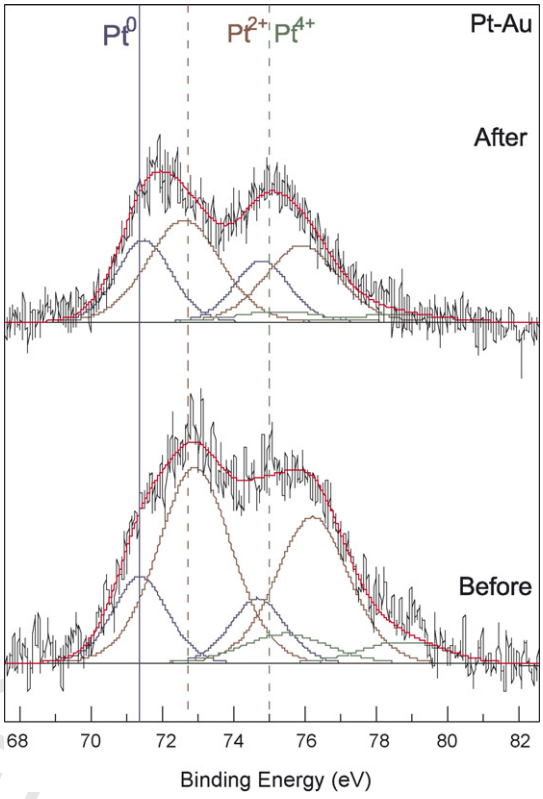

Fig. 9. Pt-4f core-level region of the Pt-Au sample before (bottom) and after (top) reaction with MeOH. Temperature during the reaction ranged from 100 to 300 °C with a total time on-stream of ~8 h.

Pt atoms (versus atoms from the less active secondary metal, M) at the NP surface in these samples. A more detailed study of the reactivity of pure Pt NPs with different Pt-oxide concentrations is currently being conducted in our group in order to shed light on this open question.

Finally, as was mentioned in the introduction, we would like to highlight that the choice of oxide support is crucial in the stability of surface and subsurface oxides on supported metal nanoparticles. For example, our group has observed faster and lower temperature PtO_x and Au_2O_3 reductions on pre-oxidized Pt and Au clusters deposited on TiO_2 as compared to the higher stability observed when ZrO_2 and SiO_2 substrate were considered [50,102].

4.2. Segregation

Reactor data (Fig. 6), in conjunction with XPS (Fig. 3) data, lead us to a model of segregation in our Pt-M samples, dictated largely by the affinity of metal M for oxygen. In Fig. 10 we present a simplified scheme of this model showing truncated, faceted NPs in contact with the ZrO_2 support. The light circles represent Pt atoms and the dark circles represent the atoms of the secondary metal M. The Pt-Au sample, Fig. 10(a), appears to be the most homogeneous alloy of all our samples. This is due to a combination of Au's favorable surface segregation (thermodynamic) properties attenuated by Pt's higher affinity for oxygen. The remaining samples have a segregation trend that follows the same line of reasoning, where the expected segregation due to lower surface energy, higher atomic volume, heats of sublimation, etc. are overcome by metal M's favorable interaction with oxygen during the process of sample annealing in air. Fig. 10(b) shows the Pt-Pd and Pt-Ru to have a Pt-rich core and Fig. 10(c) includes most of the Fe in the Pt-Fe at the NP surface. In addition to this scheme, as previously

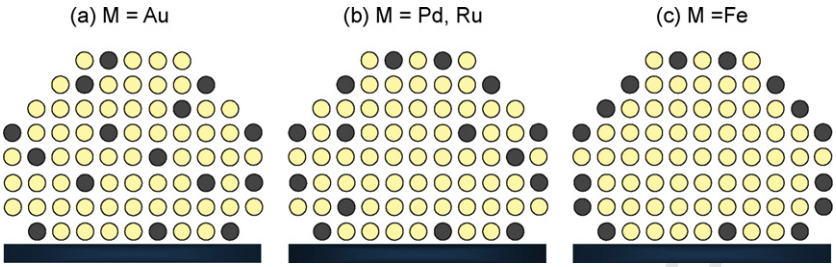

Fig. 10. Simplified cross sectional schematic of surface segregation phenomena in Pt-M alloys where the oxygen affinity of metal M dominates its distribution within the segregation profile. Image (a) represents the homogeneous Pt-Au alloy, (b) Pt-Pd and Pt-Ru, and (c) Pt-Fe. Light circles represent Pt atoms and dark circles represent the metal M.

discussed, there may exist regions or patches of different species (Pt^0, PtO_x, M^0, MO_x) in contact with each other at the NP surface. These boundaries may enhance interactions with the gas-phase reactants and/or products. Future research on the reactivity of Pt-oxides in reactions that involve oxygen (e.g. CO oxidation) should provide further insight into some of the challenging, open questions described above.

5. Conclusions

We have tested a series of monometallic (M) and bimetallic (Pt-M) nanocatalysts for the decomposition of MeOH. All catalysts had the same initial particle size distribution, support, and preparation conditions. We therefore attribute any differences in the properties of these catalysts to the addition of the secondary metals. XPS analysis reveals the most stable component of these systems to be PtO, which proves to be highly stable under our reaction conditions. XPS, in conjunction with reaction data, shows a trend relating the concentration of Pt^0 and PtO to the segregation of metal M and subsequent catalytic activity as follows. Because all samples were calcined in air, the metals with the highest affinity for oxygen tended to surface segregate in the Pt-M NPs. This directly affected the NP's catalytic activity by way of metal M's occupation of surface sites available for reaction with MeOH and possibly through its influence on the oxidation state of Pt.

We hope this study will stimulate further theoretical investigations on the effect of the chemical environment on segregation phenomena at the nanoscale, as well as on the activity and stability of Pt-oxides as a function of metal dopants in bimetallic systems.

Acknowledgments

We would like to thank Prof. Perla Balbuena (Texas A&M) and Prof. Werner Keune (Univ. Duisburg-Essen) for helpful discussions. This work has been partially supported by the US Department of Energy (DE-FG02-08ER15995). Funding from the Donors of the American Chemical Society Petroleum Research Fund (supplement to grant PRF-42701-G5 for minority undergraduate summer research) and the National Science Foundation (NSF-REU, EEC 0453436) is greatly appreciated.

References

[1] N.M. Markovic, T.J. Scmidt, V. Stamenkovic, P.N. Ross, Fuel Cells 1 (2001) 105.
[2] F. Wu, H. Murakami, Y. Yamabe-Mitarai, H. Harada, H. Katayama, Y. Yamamoto, Surf. Coat. Technol. 184 (2004) 24.
[3] J.R. Rostrup-Nielsen, Phys. Chem. Chem. Phys. 3 (2001) 283.
[4] Y. Xu, A.V. Ruban, M. Mavrikakis, J. Am. Chem. Soc. 126 (2004) 4717.
[5] U.A. Paulus, A. Wokaun, G.G. Scherer, T.J. Schmidt, V. Stamenkovic, N.M. Markovic, P.N. Ross, Electrochim. Acta 47 (2002) 3787.
[6] S. Mukerjee, S. Srinivasan, M.P. Soriaga, J. Mcbreen, J. Electrochem. Soc. 142 (1995) 1409.
[7] V.A. Lubarda, Mech. Mater. 35 (2003) 53.
[8] P.L. Hansen, A.M. Molenbroek, A.V. Ruban, J. Phys. Chem. B 101 (1997) 1861.
[9] D.R. Rolison, P.L. Hagans, K.E. Swider, J.W. Long, Langmuir 15 (1999) 774.
[10] S. Shukla, S. Seal, Nanostruct. Mater. 11 (1999) 1181.
[11] J. Zhang, F.H.B. Lima, M.H. Shao, K. Sasaki, J.X. Wang, J. Hanson, R.R. Adzic, J. Phys. Chem. B 109 (2005) 22701.
[12] G.F. Wang, M.A. Van Hove, P.N. Ross, M.I. Baskes, Prog. Surf. Sci. 79 (2005) 28.
[13] Z.H. Gu, P.B. Balbuena, J. Phys. Chem. C 112 (2008) 5057.
[14] G.E. Ramirez-Caballero, P.B. Balbuena, Chem. Phys. Lett. 456 (2008) 64.
[15] T. Toda, H. Igarashi, M. Watanabe, J. Electroanal. Chem. 460 (1999) 258.
[16] H. Igarashi, T. Fujino, Y.M. Zhu, H. Uchida, M. Watanabe, Phys. Chem. Chem. Phys. 3 (2001) 306.
[17] S. Desai, M. Neurock, Electrochim. Acta 48 (2003) 3759.
[18] Q. Yi, A. Chen, W. Huang, J. Zhang, X. Liu, G. Xu, Z. Zhou 9 (2007) 1513. Q1
[19] A. Morlang, U. Neuhausen, K.V. Klementiev, F.W. Schutze, G. Miehe, H. Fuess, E.S. Lox, Appl. Catal. B-Environ. 60 (2005) 191.
[20] W. Rachmady, M.A. Vannice, J. Catal. 209 (2002) 87.
[21] M. Bowker, T. Aslam, M. Roebuck, M. Moser, Appl. Catal. A 257 (2004) 57.
[22] S.E. Maisuls, K. Seshan, S. Feast, J.A. Lercher, Appl. Catal. B 29 (2001) 69.
[23] K.K. Bando, T. Kawai, K. Asakura, T. Matsui, L. Le Bihan, H. Yasuda, Y. Yoshimura, S.T. Oyarna, Catal. Today 111 (2006) 199.
[24] J.R. Kitchin, N.A. Khan, M.A. Barteau, J.G. Chen, B. Yakshinksiy, T.E. Madey, Surf. Sci. 544 (2003) 295.
[25] K. Endo, K. Nakamura, Y. Katayama, T. Miura, Electrochim. Acta 49 (2004) 2503.
[26] A. Niquille-Rothlisberger, R. Prins, Catal. Today 123 (2007) 198.
[27] D.A. Simonetti, E.L. Kunkes, J.A. Dumesic, J. Catal. 247 (2007) 298.
[28] O.S. Alexeev, G.W. Graham, M. Shelef, B.C. Gates, J. Catal. 190 (2000) 157.
[29] F. Donsi, K.A. Williams, L.D. Schmidt, Ind. Eng. Chem. Res. 44 (2005) 3453.
[30] R.D. Cortright, P.E. Levin, J.A. Dumesic, Ind. Eng. Chem. Res. 37 (1998) 1717.
[31] W. Huang, J.R. McCormick, R.F. Lobo, J.G. Chen, J. Catal. 246 (2007) 40.
[32] M. Englisch, V.S. Ranade, J.A. Lercher, J. Mol. Catal. A 121 (1997) 69.
[33] R.W.J. Scott, A.K. Datye, R.M. Crooks, J. Am. Chem. Soc. 125 (2003) 3708.
[34] N. Taylor, H. Kim, J.E. Greene, Surf. Sci. 475 (2001) 171.
[35] T.N. Taylor, C.T. Campbell, Surf. Sci. 280 (1993) 277.
[36] J.A. Rodriguez, C.M. Truong, D.W. Goodman, Surf. Sci. 271 (1992) L331.
[37] R. Zeis, A. Mathur, G. Fritz, J. Lee, J. Erlebacher, J. Power Sources 165 (2007) 65.
[38] Y.H. Niu, R.M. Crooks, C.R. Chim. 6 (2003) 1049.
[39] Y. Shu, L.E. Murillo, J.P. Bosco, W. Huang, A.I. Frenkel, J.G. Chen, Appl. Catal. A 339 (2008) 169.
[40] J.C. Serrano-Ruiz, G.W. Huber, M.A. Sanchez-Castillo, J.A. Dumesic, F. Rodriguez-Reinoso, A. Sepulveda-Escribano, J. Catal. 241 (2006) 378.
[41] O. Ozturk, J.B. Park, S. Ma, J.S. Ratliff, J. Zhou, D.R. Mullins, D.A. Chen, Surf. Sci. 601 (2007) 3099.
[42] H.B. Zhao, B.E. Koel, J. Catal. 234 (2005) 24.
[43] N.A. Zarkevich, T.L. Tan, D.D. Johnson, Phys. Rev. B 75 (2007).
[44] A.L. Bonivardi, F.H. Ribeiro, G.A. Somorjai, J. Catal. 160 (1996) 269.
[45] T. Ruhle, et al. Appl. Catal. B 14 (1997) 69.
[46] D. Fliegel, Z. Berner, D. Eckhardt, D. Stuben, Anal. Bioanal. Chem. 379 (2004) 131.
[47] M. Peuckert, H.P. Bonzel, Surf. Sci. 145 (1984) 239.
[48] M. Schmid, S. Zimmermann, H.F. Krug, B. Sures, Environ. Int. 33 (2007) 385.
[49] J.R. Croy, S. Mostafa, J. Liu, Y.H. Sohn, B. Roldan Cuenya, Catal. Lett. 118 (2007) 1.
[50] J.R. Croy, S. Mostafa, J. Liu, Y.H. Sohn, H. Heinrich, B. Roldan Cuenya, Catal. Lett. 119 (2007) 209.
[51] B.L.M. Hendriksen, J.W.M. Frenken, Phys. Rev. Lett. 89 (2002).
[52] W. Li, B. Hammer, Chem. Phys. Lett. 409 (2005) 1.
[53] J.P. Spatz, S. Mossmer, C. Hartmann, M. Möller, T. Herzog, M. Krieger, H.G. Boyen, P. Ziemann, B. Kabius, Langmuir 16 (2000) 407.
[54] B. Roldan Cuenya, S.H. Baeck, T.F. Jaramillo, E.W. McFarland, J. Am. Chem. Soc. 125 (2003) 12929.
[55] L.K. Ono, D. Sudfeld, B.R. Cuenya, Surf. Sci. 600 (2006) 5041.
[56] B.V. Crist, Handbook of Monochromatic XPS Spectra—Commercially Pure Binary Oxides, vol. 2, XPS International, Inc., 2005,, p. 828.
[57] W.B. Pearson (Ed.), A Handbook of Lattice Spacings and Structures of Metals and Alloys, vol. 1, Perfamon, Oxford, 1964.
[58] W.B. Pearson (Ed.), A Handbook of Lattice Spacings and Structures of Metals and Alloys, vol. 2, Pergamon, Oxford, 1967.
[59] NIST X-ray Photoelectron Spectroscopy Database, Version 3.4 (Web Version) http://srdata.nist.gov/xps/index.htm.
[60] A.S. Arico, A.K. Shukla, H. Kim, S. Park, M. Min, V. Antonucci, Appl. Surf. Sci. 172 (2001) 33.

[61] A.K. Shukla, M. Neergat, P. Bera, V. Jayaram, M.S. Hegde, J. Electroanal. Chem. 504 (2001) 111.
[62] J.L.G. Fierro, J.M. Palacios, F. Tomas, Surf. Interface Anal. 13 (1988).
[63] A. Howard, D.N.S. Clark, C.E.J. Mitchell, R.G. Egdell, V.R. Dhanak, Surf. Sci. 518 (2002) 210.
[64] R. Symanski, H. Charcosset, Platinum Met. Rev. 30 (1986) 23.
[65] P. Oelhafen, J. Phys. F: Met. Phys. 11 (1981) L41.
[66] L.K. Ono, J.R. Croy, B. Roldan Cuenya, in press.
[67] G.V. Samsonov (Ed.), The Oxide Handbook, second ed., Plenum Publishing Corporation, New York, 1982.
[68] E. Antolini, T. Lopes, E.R. Gonzalez, J. Alloys Compd. 461 (2008) 253.
[69] J.W. Arblaster, Platinum Met. Rev. 51 (2007) 130.
[70] C. Creemers, P. Deurinck, Surf. Interface Anal. 25 (1997) 177.
[71] K.F. Wojciechowski, Surf. Sci. 437 (1999) 285.
[72] D.S. Mainardi, P.B. Balbuena, Langmuir 17 (2001) 2047.
[73] B.E. Nieuwenhuys, Adv. Catal. 144 (2000) 259.
[74] L. Guczi, Catal. Today 101 (2005) 53.
[75] Y.G. Ma, P.B. Balbuena, Surf. Sci. 602 (2008) 107.
[76] E. Irissou, M.C. Denis, M. Chaker, D. Guay, Thin Solid Films 472 (2005) 49.
[77] Z. Bastl, T.P. Pick, Surf. Sci. 566 (2004) 832.
[78] J. Zhang, K. Sasaki, E. Sutter, R.R. Adzic, Science 315 (2007) 220.
[79] U.B. Demirci, J. Power Sources 173 (2007) 11.
[80] J.W. Niemantsverdriet, J.A.C. van Kaam, C.F.J. Flipse, A.M. van der Kraan, J. Catal. 96 (1985) 58.
[81] G.W. Graham, H.W. Jen, O. Ezekoye, R.J. Kudla, W. Chun, X.Q. Pan, R.W. McCabe, Catal. Lett. 116 (2007) 1.
[82] R. Lopez, R. Romero, F. Martin, J.R. Ramos-Barrado, D. Leinen, Surf. Interface Anal. 38 (2006) 277.
[83] P. Waszczuk, G.Q. Lu, A. Wieckowski, C. Lu, C. Rice, R.I. Masel, Electrochim. Acta 47 (2002) 3637.
[84] J. Greeley, J.K. Norskov, M. Mavrikakis, Annu. Rev. Phys. Chem. 53 (2002) 319.
[85] R. Blume, M. Havecker, S. Zafeiratos, D. Teschner, A. Knop-Gericke, R. Schlögl, P. Dudin, A. Barinov, M. Kiskinova, Catal. Today 124 (2007) 71.
[86] J.R. Croy, S. Mostafa, B. Roldan Cuenya, in press.
[87] H. Iida, A. Igarashi, Appl. Catal. A 303 (2006) 192.
[88] P. Bera, S. Malwadkar, A. Gayen, C.V.V. Satyanarayana, B.S. Rao, M.S. Hegde, Catal. Lett. 96 (2004) 213.
[89] N. Seriani, W. Pompe, L.C. Ciacchi, J. Phys. Chem. B 110 (2006) 14860.
[90] J.M. Petroski, Z.L. Wang, T.C. Green, M.A. El-Sayed, J. Phys. Chem. B 102 (1998) 3316.
[91] N. Seriani, F. Mittendorfer, J. Phys. Condens. Mater. 20 (2008).
[92] Y. Abe, M. Kawamura, K. Sasaki, Jpn. J. Appl. Phys. 1 (38) (1999) 2092.
[93] J.G. Wang, W.X. Li, M. Borg, J. Gustafson, A. Mikkelsen, T.M. Pedersen, E. Lundgren, J. Weissenrieder, J. Klikovits, M. Schmid, B. Hammer, J.N. Andersen, Phys. Rev. Lett. 95 (2005) 256102.
[94] J.F. Weaver, J.J. Chen, A.L. Gerard, Surf. Sci. 592 (2005) 83.
[95] C.B. Wang, C.T. Yeh, J. Catal. 178 (1998) 450.
[96] W. Wen, J. Rodriguez, J. Croy, S. Mostafa, B. Roldan Cuenya, in press.
[97] Y. Xu, J. Greeley, M. Mavrikakis, J. Am. Chem. Soc. 127 (2005) 12823.
[98] A.F. Carley, A.W. Owens, M.K. Rajumon, M.W. Roberts, S.D. Jackson, Catal. Lett. 37 (1996) 79.
[99] S.T. Yong, K. Hidajat, S. Kawi, Catal. Today 131 (2008) 188.
[100] I.E. Wachs, R.J. Madix, J. Catal. 53 (1978) 208.
[101] X. Wang, W.K. Chen, C.H. Lu, Appl. Surf. Sci. 254 (2008) 4421.
[102] L.K. Ono, B. Roldan Cuenya, J. Phys. Chem. C 112 (2008) 4676.

Please cite this article in press as: J.R. Croy, et al., Appl Catal A: Gen (2008), doi:10.1016/j.apcata.2008.08.013